1_C8

CFD Simulations Of An Aerosol Chamber For Calibration Of Low-Cost Particulate Matter Sensors

Jan Drzymalla, MEng *Student Member ASHRAE*
Yannic Lay, BEng
Marc Sauermann, BEng
Andreas Henne, DrIng

ABSTRACT

Due to the negative effects of Particulate Matter exposure, more and more inexpensive optical aerosol spectrometers and photometers (low-cost PM sensors) are coming to the market, which are often used to monitor air quality. In addition to the low acquisition costs, these commercial PM sensors are characterized by low maintenance effort, which enable very high data availability in continuous operation. However, questions about the quality of the generated data often remain unanswered. To investigate the data quality and measurement accuracy of low-cost PM sensors, comparative measurements with reference devices within aerosol chambers are suitable. Aerosol chambers offer protection from external influences, provide adjustable test environments and can therefore be enormously helpful in calibrating measuring instruments. However, these chambers are not yet standardized, making computational fluid dynamics (CFD) the obvious choice for obtaining certainty about their usefulness and flow behavior. Accordingly, a prototype aerosol chamber (0.16 m³) was developed and its fluid dynamics were investigated using CFD in this parameter study. The primary goal was the optimization of the chamber geometry and the associated components such as inlet and outlet openings as well as flow straighteners in order to form a laminar flow in the test area that was distributed as evenly as possible. The simulation was performed with ANSYS Fluent 2019 R2 using the dense discrete phase model, which is a hybrid euler-lagrange approach. The gas phase (air) was modeled with the euler approach and the particle phase with the lagrange approach. The particle phase was based on a polydisperse calcium carbonate powder (ϱ = 2.7 g/ml) with particle diameters from 1 to 21 μm. Results of the study include geometric optimizations of the aerosol chamber, predicted flow pattern of air velocity, predicted particle trajectories and localization of a calibration zone.

INTRODUCTION

The increasing fine dust pollution in large cities is a health hazard for the people living there. Smart Buildings are able to measure this pollution so that the air quality can be constantly monitored to achieve the highest possible air quality in the building (X. Chen et al. 2014). The required sensors must be financially economical and also sufficiently precise. In recent years, the number of low-cost particulate matter sensors (low-cost PM sensors) available on the market has increased noticeably, but it can be assumed that they do not meet the quality criteria of scientific or suitability-tested measurement technology (Asbach et al. 2018). Accordingly, careful calibrations are necessary, which ultimately enable the use for new applications. The first step in calibration is to determine a relationship between a measured value and the true value. In a second step, this information is used to derive the true values from the measured values (Deutsches Institut für Normung e. V. 1995; International Bureau of Weights and Measures 2008). Measuring devices can be calibrated using empirical methods or theories based on the laws of nature. These theories describe the behaviour of the measuring devices so that a prediction of the measurement result is possible. Theoretical calibrations may not take into account all effects that occur in reality, which can lead to deviating references. In empirical measurements, on the other hand, deviating reference values also occur, which cause unequal boundary conditions during calibration in test setups (Cheng and B. T. Chen 2008). This typically refers to measurements under real conditions, where an attempt is made to

Jan Drzymalla is a research associate at the Institute of Building Services Engineering, University of Applied Sciences (TH Köln), Cologne, Germany. **Yannic Lay** and **Marc Sauermann** are master's students in the Department of Plant, Energy and Machine Systems, University of Applied Sciences (TH Köln), Cologne, Germany. **Andreas Henne** is a professor at the Institute of Building Services Engineering, University of Applied Sciences (TH Köln), Cologne, Germany.

avoid disturbance variables (e.g. direct pollutants or heat sources, and ventilation openings) (Moreno-Rangel et al. 2018). Often, the supposed disturbance variables are not analyzed in more detail, which can lead to misjudgments as a result (Demanega et al. 2021). Furthermore, low-cost PM sensors often do not have an intake manifold that allows direct calibration via tube. Accordingly, the use of measuring chambers is essential for the empirical calibration of low-cost PM sensors. This allows test environments to be created in which the interior of the system is shielded from external influences. Thus, disturbance variables can be reduced and conditions such as a changed pressure or temperature can be created or maintained inside the chamber. The relevant particles for the calibration of particle measuring devices can be provided in the form of an aerosol as a mixture of a test dust and air and fed into the system via an inlet. A uniform distribution of the test aerosol can be ensured, for example, by using atomizers or aerosol generators. To achieve a continuous particle concentration in the system, outlets can be installed to transport the aerosol out of the measuring chamber via pressure equalization or ventilation. Depending on the geometric design of a measuring chamber, occurring flows or turbulences can be changed or prevented by additional geometric elements such as laminarisators or guiding geometries (Hapidin et al. 2019; Feather and B. T. Chen 2003; Cheng and B. T. Chen 2008). As there are no uniformly standardized aerosol measuring chambers available so far, both the flow and particle behavior within the chambers are unknown. Therefore, this study is dedicated to the fluidic investigation of an existing aerosol measuring chamber, which will be used for the calibration of low-cost PM sensors. For this purpose, different air and particle flow simulations are performed on the existing chamber geometry using the computational fluid dynamics (CFD) capable software solution ANSYS Fluent. The aim is to optimize the existing chamber geometry in terms of flow and to define a potential calibration zone within it. These results shall be used to enable a uniformly distributed aerosol flow in a calibration zone yet to be defined, so that constant aerosol concentrations prevail in comparative measurements.

METHOD AND MATERIALS

In this section, the methodical procedure is explained to investigate the flow dynamics within aerosol measuring chambers by means of CFD simulations. In the following, the applied modeling approach as well as the boundary conditions to be considered within the simulation software are described. Finally, the aerosol chamber to be investigated and its design is explained in more detail.

Modeling Approach

For the fluidic investigation of the aerosol chamber, different steps have to be passed through, which are shown schematically in Figure 1. In the first step the existing initial geometry of the aerosol measuring chamber has to be modeled with a digital modeling tool. During the modeling process, 3D geometries have to be created as solids and 2D geometries as one continuous region. Unimportant geometry parts should be represented in a simplified way as far as possible in order to save computing time and capacity in later calculation or simulation steps. Once the computer-aided design (CAD) model is completed, it can be exported and in a second step imported into a CFD software. Within this software environment the CAD model must be prepared in the internal design modeler. This includes the selection of preferred length units and the creation of component groups. The latter serves to combine individual solids into an assembly if several solids or regions are imported via the CAD file. If this step is not carried out, adjacent solids/regions are not considered to be connected afterwards. Moreover, these must be named and declared as solid or fluid spaces. Step 3 is about the meshing of the geometry, which has an enormous influence on the simulation accuracy and duration. During meshing, the existing geometry is divided into smaller parts, which are called elements (AUTODESK Inc. 2019). The existing corners of each element are called nodes at which the simulation calculation is performed. The individual nodes and elements together form the geometry mesh. Both the solid and fluid spaces have to be meshed by declaring all geometry surfaces. This means, for example, the definition of inlet, outlet or symmetry surfaces. After the surface declaration, the mesh type is selected, whereby a distinction must be made between structured and unstructured meshes (Sturm 2019). If possible, structured meshes like hexadrons should be chosen, because they have a higher mesh quality, a higher numerical model accuracy and a shorter calculation time compared to unstructured meshes like tetrahedrons or polyhedrons (Sturm 2019). Furthermore, the mesh quality can be determined via the orthogonal quality, aspect ratio

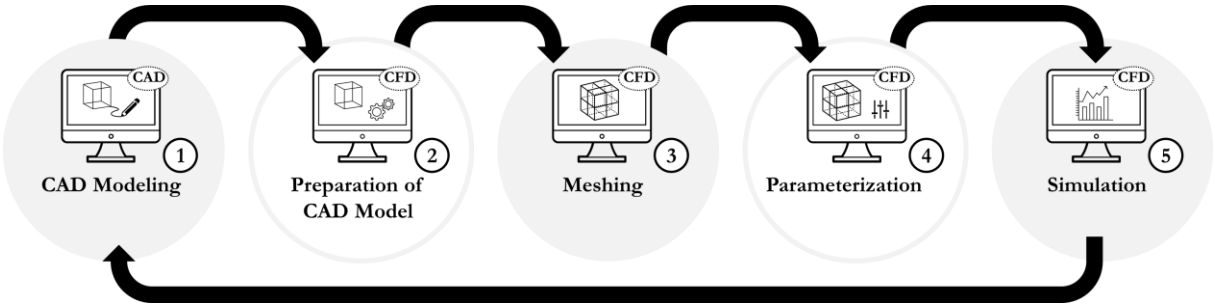

Figure 1 Schematic workflow of the modeling approach.

and skewness. When choosing the mesh, the accuracy, efficiency and simplicity of generation should be weighed against each other. After the geometry has been successfully meshed, the parameterization is carried out in Fluent in step 4. In the first step of the parameterization, the mesh is checked, including domain extents, volume statistics, mesh topologies and node positions (ANSYS Inc. 2020a). Once the grid check has been completed without problems, the actual parameterization can begin. This includes the choice between pressure- and density-based solver methods. Then it is selected whether the simulation should be stationary or transient. To find out whether a steady or transient problem exists, a steady simulation can be carried out first, followed by a transient simulation without initialization. If time-dependent changes can be seen in the contour plots, then there is a transient problem. In addition, the gravitational force of the respective geometric axis must be considered and suitable flow models must be selected. For the investigation of particle flows, the eulerian multiphase model in combination with the dense discrete phase model (DDPM) is a preffered choice. In the hybrid euler-lagrange approach, the gas phase is modelled with the euler approach and the particle phase with the lagrange approach. In addition, a viscous model should be used for laminar, turbulent or inviscid flows. Once the model selection is complete, the properties of the solid and fluid materials must be defined. In particle simulation, this is done by first defining the discrete phase, which is injected into the system. Localization as well as the type and manner of injection in the simulation model can be defined more precisely via the injection type. The injection is performed via the geometrically simplified nozzle. The particle type to be injected is defined as "inert-type", because the particle mass has a relevant influence in the simulation model and thus on the result. The test aerosol to be simulated must also be mapped correctly. For this purpose, the Rosin, Rammler, Sperling & Bennet (RRSB) distribution, which can be defined within Fluent, is used. The RRSB distribution offers a realistic representation of the test aerosol by formulating the mass distribution and is calculated according to equation 1 as follows (ANSYS Inc. 2020b):

$$Y_d = e^{-\left(\frac{d}{d_{mean}}\right)^n} \quad (1)$$

For the calculation of the mass distribution according to RRSB in Fluent, the maximum, minimum and mean particle size (d_{max}, d_{min} & d_{mean}) must be given in micrometer. In addition, information on the number of diameters (N_d) and the spread parameter (n) must be provided. Furthermore, for the injection of the discrete phase a volume flow and an inlet velocity is defined with which the particles enter the system. Subsequently, the materials used for the chamber geometry and components must be defined and then assigned to the individual volume bodies. Once the steps described above have been carried out, the under-relaxation factors, e.g. for pressure and momentum, can be easily adjusted to stabilize the simulation model. The calculation should always be monitored by various monitoring of selected parameters over the calculation/iteration period. For example, the residuals, flow velocities or mass flows can be continuously evaluated. For the optimization of the aerosol chamber, the five methodical steps must be iteratively run through until the desired result is achieved. At the beginning, air flow simulations are carried out to make initial geometric optimizations. Particle flow simulations follow, on the basis of which the final aerosol chamber is designed and a calibration zone is defined.

Aerosol Chamber Setup

The existing aerosol chamber is a chamber geometry of about 0.16 m³ which is shown in figure 2 and was modeled with Autodesk AutoCAD. There, a two-dimensional CAD section (see figure 2a) can be seen, where different components (see Figure 2b) are highlighted in different colours. The modeled chamber enclosure surfaces are shown in orange

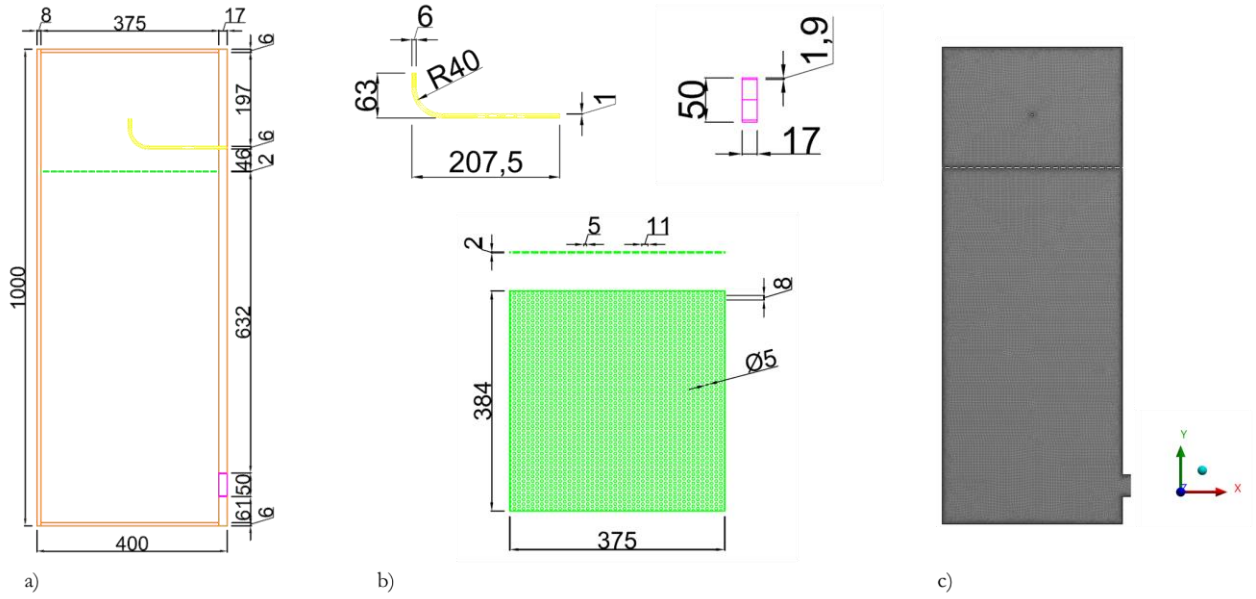

Figure 2 Geometry a) of the prototype aerosol chamber, b) of the components and c) grid used in the CFD simulations (dimensions in mm).

and consist of glass. Only the 17 mm thick wall is a coated chipboard to allow for inlet and outlet holes. The air or aerosol inlet is an aluminium tube with an outer diameter of 6 mm and a wall thickness of 1 mm. In addition, the end of the tube is bent within the chamber in a radius of 40 mm so that the incoming aerosol is directed against the chamber ceiling. In the future, this guide tube is to be connected to an aerosol generator, whereby a test aerosol is transported into the chamber at an isothermal inlet velocity. The aerosol is to be directed against the chamber ceiling in order to create a uniform particle distribution within the chamber. The aerosol shall then be passed through a straightener to laminarize the particle flow. A 2 mm thick aluminium RV5-8 perforated plate is provided for this purpose. In addition, an outlet opening is placed in the lower part of the chamber to allow natural pressure equalization. In addition, Figure 2c illustrates the CFD model linked with ANSYS on which the air flow simulations are carried out. Here it can be seen that the outer walls were not considered in the CFD model because they are irrelevant for the fluid flow. Furthermore, the inlet pipe was modeled in a simplified way, because otherwise the entire pipe section would represent a non-penetrable layer in a two-dimensional section. Table 1 lists the basic parameters used for meshing and air flow simulations

Table 1. Meshing and Model Parameter in ANSYS (Air)

Global Element Size	Mesh Type	Node Value	Setup	Turbulence Model	Phase	Solution Method
3 mm	Triangular/Square	88,944	Pressure-Based, Steady	Standard k-epsilon	Phase 1: Air	SIMPLE

in ANSYS. It can be seen that the aerosol chamber was meshed with a global mesh size of 3 mm, using a combined method of triangular and square cells. In addition, several prismatic layers on the outer walls, at the straightener and at the inlet were generated with a mesh size of 1 mm. The generated mesh thus creates 88,944 nodes which have to be passed through during the simulation. The standard k-epsilon turbulence model and the standard wall functions are used for the air flow simulations to be performed in ANSYS Fluent. Furthermore, the flow problems are solved stationary, with the pressure-based solver using the SIMPLE method. For particle flow simulations, on the other hand, an optimized geometry is used, which results from the air flow simulations described above. In addition, the simulation boundary conditions, which are largely listed in Table 2, must be adapted. Using the specified boundary conditions and the Phase Coupled SIMPLE method, $CaCO_3$ particles are simulated over a 10-second injection.

Table 2. Meshing and Model Parameter in ANSYS (Mixture)

Global Element Size	Mesh Type	Setup	Multiphase	Turbulence Model	Phase	RRSB
3 mm	Triangular/Square	Pressure-Based, Transient	Eulerian DDPM	RNG k-epsilon	Phase 1: Air Phase 2: $CaCO_3$ (ϱ = 2.7 g/ml)	d_{min} = 1 µm d_{max} = 21 µm d_{mean} = 5 µm n = 1.96 N_d = 10

RESULTS

In a first series of preliminary investigations, the air flow within the aerosol chamber described above was examined. For this purpose, inlet velocities between 1 m/s and 6 m/s were varied and compared at three different chamber heights. These areas were investigated as possible calibration zones where the low-cost PM sensors to be calibrated could be placed in the future. The preferred aerosol generator works with volume flows between 200 l/h and 250 l/h, which results in approximate inlet velocities of 4.42 m/s to 5.53 m/s at an inlet diameter of 4 mm. This velocity range is therefore decisive for the selection of the calibration zone. Figure 3a shows two contours of the velocity magnitude at an inlet velocity of 5 m/s. The first contour (left) clearly shows how the air flows upwards and is evenly distributed on both sides of the chamber near the ceiling. In this area the highest flow velocities and a maximum cell reynolds number of 280 occur. Since the reynolds numbers are well below 2300, a laminar flow can be assumed. Towards the bottom of the chamber the flow velocity tends to decrease further, so that differences in velocity in the standard resolution are hardly visible graphically. Accordingly, in Figure 3a (right) the resolution was increased by reducing the maximum air velocity to be displayed to 0.1 m/s. This shows that the flow velocities increase slightly again near the outlet opening. In addition, a kind of dead space is formed in the lower left-hand corner of the chamber, in which the air comes to a nearly complete standstill. This could lead to the fact that aerosol particles are deposited there more and more and are no longer led out of the chamber. On the other hand, at the chamber heights shown at 200 mm, 400 mm and 600 mm distance from the ground, very slow air velocities in the range of about 0.04 m/s to 0.07 m/s can be observed. The corresponding flow profiles are shown in Figure 3b, where the velocity magnitude is plotted over the chamber width. The chamber extends from -0.1875 m to 0.1875 m and has its center at zero point at X = 0 m. This X-Y plot shows that the outlet opening clearly influences the flow profile at a height of 200 mm and that a velocity difference of about 40 % can be determined between the points -0.12 m and 0.12 m. In contrast, at a distance of 400 mm and 600 mm, an almost uniform velocity magnitude of about 0.055 m/s could be determined across the entire chamber width. However, this velocity magnitude decreases slightly towards the chamber walls. These velocity profiles were then recorded at varying inlet velocities and are shown in Figures 3c to 3e. The curves shown in red represent the profiles in Figure 3b at an

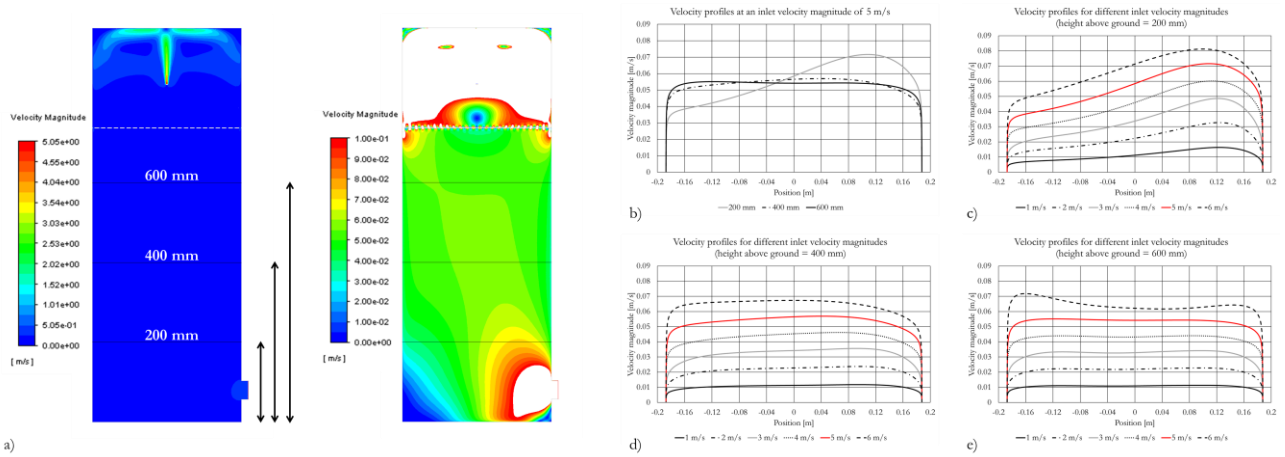

Figure 3 Contours a) of velocity magnitude and b) velocity profiles at an inlet velocity magnitude of 5 m/s, and velocity profiles for different inlet velocity magnitudes at c) 200 mm, d) 400 mm and e) 600 mm above chamber ground.

inlet velocity of 5 m/s. Even if the inlet velocities are varied, the velocity profiles remain similar at the respective chamber heights. A calibration of low-cost PM sensors at a chamber height of 200 mm is not recommended with the current chamber geometry, since the outlet opening strongly affects the velocity profile. At inlet velocities above 5 m/s, a slightly distorted velocity profile also occurs at a height of 600 mm, as shown in Figure 3e. However, if the inlet velocity is ≤ 5 m/s, the air velocities are predominantly evenly distributed over the entire chamber width. Without changing the chamber geometry, a calibration zone at a distance of 400 mm from the ground is therefore preferable from a fluidic point of view. In a second step, different chamber geometries and components were fluidically investigated in order to optimize the existing Aerosol chamber. In Figure 4, four simulated chamber variants are presented, where an inlet velocity of 5 m/s was set. In order to be able to compare the results with the initial geometry from Figure 3a, the resolution of the air velocity was limited to a maximum of 0.1 m/s and the evaluation lines were drawn in 200 mm, 400 mm and 600 mm height. In Figure 4a, the flow velocity was investigated for a chamber without the use of a straightener. Compared to the initial geometry, a much more turbulent flow pattern is created without the flow straightener. Thus, flow velocities of 0.1 m/s are already achieved at a height of 400 mm and 600 mm, which were previously prevented by the straightener. This proves that a straightener can reduce the flow velocities within the chamber and distribute them more evenly. For this reason, a straightener will continue to be used for the optimized aerosol chamber. In contrast, Figure 4b simulates the air velocity when the aerosol chamber is reduced by a third. The flow pattern is similar to that of Figure 3a with the difference that the flow-calmed zone between 400 mm and 600 mm and the evenly distributed velocity profile of 0.055 m/s (see Figure 3d,e) is omitted. If the outlet opening is also changed in this geometry variant (see Figure 4c), the formation of dead spaces in the chamber ground corners can be prevented, but this reinforces the unevenly distributed velocity profile at 200 mm and 400 mm height. In the end, the most advantageous geometry from a fluidic point of view is the initial geometry with a centrally placed outlet opening in the floor (see Figure 4d). This allowed an almost symmetrical flow pattern to be created on both sides of the chamber and prevented dead spaces in the chamber corners. A calibration of low-cost PM sensors is also possible with this variant in a chamber height of 400 mm, because the flow behaves almost identically over the entire chamber width. In this range the reynolds number is between 0.16 and 0.005 at a maximum velocity of 0.055 m/s. This is to ensure that the low-cost PM sensor and reference device are exposed to the same flow and aerosol concentration. In the last step, a 10-second particle flow simulation was carried out on the optimized geometry in Figure 4d, at an inlet velocity of 5 m/s and a mass flow of 1.6941e-04 kg/s. Here, 2.1742e+11

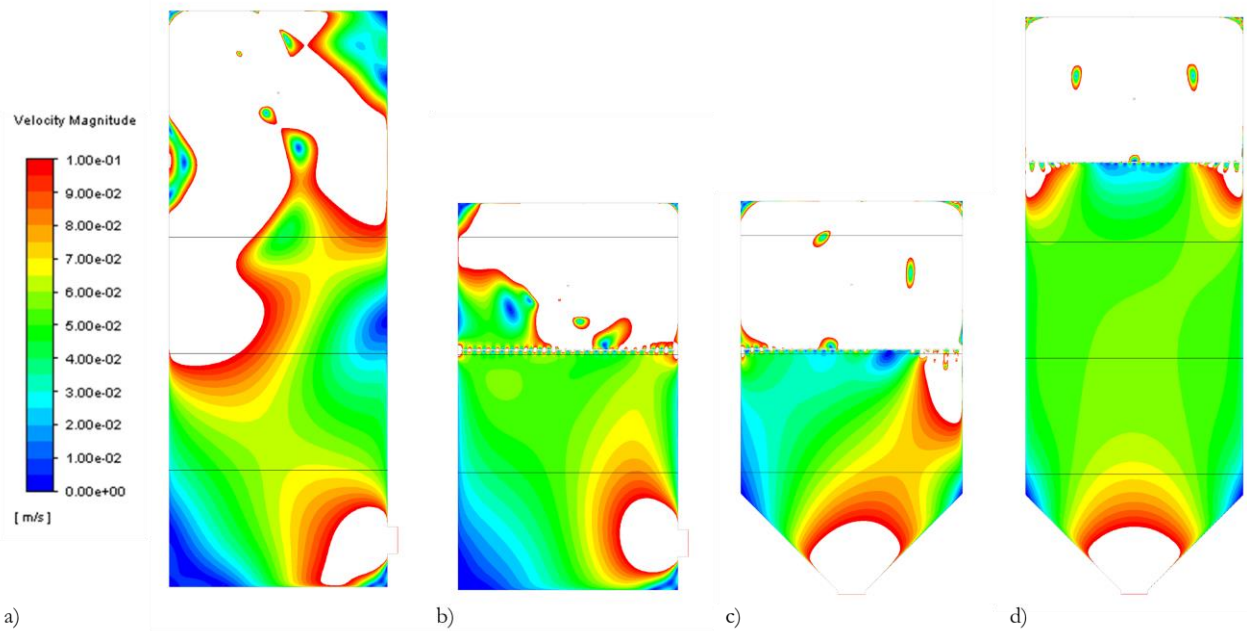

Figure 4 Contours of velocity magnitude for a a) chamber without a flow straightener, b) chamber reduced by a third, c) chamber reduced by a third with an floor outlet and d) chamber with an floor outlet at an inlet velocity magnitude of 5 m/s.

particles were simulated, corresponding to a mass of 1.6941e-03 kg. 3,631 of these particles left the chamber via the outlet after the observation period of 10 seconds. As a result, four different particle traces are shown in Figure 5. Figure 5a shows the particle traces for ten different particle diameters between 1 µm and 21 µm. Basically, the particles follow the airflow as predicted by the airflow simulations (see Figures 3a and 4d). After particle injection, two circular particle flows form above the straightener, which are separated from each other by the inlet opening. Two vortices also form below the straightener, but these do not match the results of the airflow simulations. The reasons for this are manifold, since on the one hand only a single point in time is considered in a transient simulation and on the other hand different simulation boundary conditions prevail. In addition, the simulated $CaCO_3$ particles have a different density than air and collide with each other as well as with chamber components during the simulation. Within these circularly formed eddies smaller particles occur whose diameters are predominantly ≤ 5 µm. This can be explained by the comparatively lower settling velocity and by the flow velocities (see Figure 5c). The resulting flow entrains the less massive particles and keeps them trapped in the flow. In addition, Figure 5b shows the residence time of the simulated particles. There it can be clearly seen that the mentioned particle fraction within the vortices remains in the same area for the entire simulation time. Furthermore, it can be seen that the larger particles flow faster towards the chamber outlet due to their mass (see Figure 5a). Particles near the wall, on the other hand, remain significantly shorter, since the flow velocity there is higher than in the centre of the chamber. This is due to the A-shaped flow that forms below the straightener. At a chamber height of 400 mm, a velocity of about 0.02 m/s results in the centre of the chamber. Near the chamber walls, however, maximum speeds of 0.09 m/s to 0.17 m/s can be recorded. Accordingly, the reference device and the low-cost PM sensor should be placed as centrally as possible during calibration in order to be exposed to minimum flow velocities.

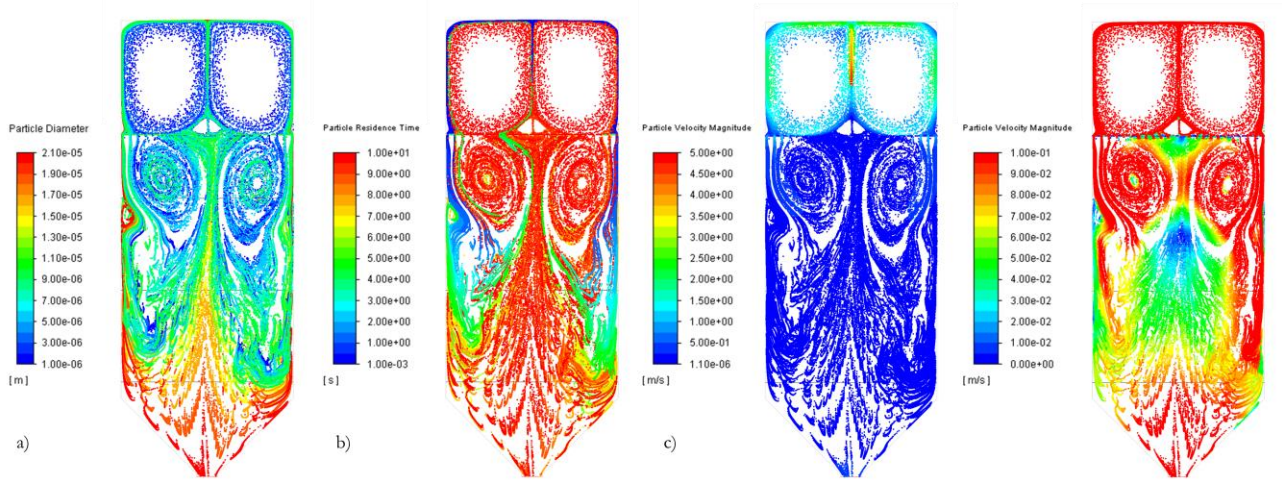

Figure 5 Particle traces colored by particle a) diameter, b) residence time and c) velocity magnitude.

CONCLUSION

On the basis of the flow simulations performed, the modified aerosol chamber shown in Figure 4d is to be preferred, where a sensor calibration is to be carried out at a height of 400 mm in the centre of the chamber if possible. It should be noted that this is only applicable if aerosol generators are used which operate with volume flows in the range between 200 l/h and 250 l/h. In addition, the results refer to a two-dimensional geometry and may deviate from reality. Accordingly, the simulation results should be validated on a three-dimensional geometry. For the time being, this was refrained from for reasons of computing capacity, but initial comparisons have shown that lower flow velocities can occur with three-dimensional geometries. Furthermore, in this study both the reference device and the sensors to be calibrated were neglected in the simulation. Depending on whether the sensors are placed inside the chamber or take in sample air from outside, the simulated flow pattern can be influenced to different intensities. Furthermore, the chamber was only examined for a single polydisperse test aerosol, which is why the results for other aerosols must be viewed critically. Since there is currently no standardized chamber design, the geometry is often adapted to the individual use case. Hence,

the chamber design presented here was also adapted for the upcoming calibration task of low-cost PM sensors. Due to the compact and very handy design of these sensors (Asbach et al. 2018), the chamber volume was deliberately kept small (0.16 m³). Compared to large chambers (Demanega et al. 2021), this has the advantage that the aerosol flowing into the chamber can be distributed fast and more homogeneously and that no additional mixing fans are needed. Furthermore, the deposition surfaces and the amount of test aerosol can be reduced. In summary, with the method described in this study a fluidic investigation of aerosol chambers is very well possible, whereby geometrical optimizations can be derived. Based on the investigations, the unknown or otherwise only imaginable flow pattern could be visualized and a calibration zone defined. Thereby, low-cost PM sensors can be calibrated optimally. Accordingly, calibration of low-cost PM sensors should be performed within aerosol chambers, as they can be used to create constant test environments that are protected from external influences. However, before building, modifying or using an aerosol chamber, the method presented should be applied. In this way, potential sources of error can be identified in preliminary stages, predictions can be made about the flow behavior, or optimizations can be made to the geometry. This can ultimately contribute to the evaluation of chamber usability and also save money and resources. Although the method presented is similar to existing solutions (Sayahi et al. 2019; Saleh 2010), it is characterized by its generally valid approach, which has been described in great detail. This allows an abstraction to any application, so that different geometries, components, environments, parameters or scenarios can be investigated and compared to each other.

REFERENCES

ANSYS Inc. 2020a. "Fluent User's Guide: 20.11. Checking the Mesh." Accessed May 24, 2020.

ANSYS Inc. 2020b. "Fluent User's Guide: 24.3.14. Using the Rosin-Rammler Diameter Distribution Method." Accessed May 24, 2020.

Asbach, Christof, Bryan Hellack, Stefan Schumacher, Michael Bässler, Michael Spreitzler, Tobias Pohl, Konradin Weber et al. 2018. "Anwendungsmöglichkeiten Und Grenzen Kostengünstiger Feinstaubsensoren." *Gefahrstoffe - Reinhaltung der Luft* (78): 242–50.

AUTODESK Inc. 2019. "Autodesk Knowledge Network: CFD - Vernetzung." Accessed April 07, 2020.

Chen, Xuxu, Yu Zheng, Yubiao Chen, Qiwei Jin, Weiwei Sun, Eric Chang, and Wei-Ying Ma, eds. 2014. *Indoor Air Quality Monitoring System for Smart Buildings: September 13 - 17, 2014, Seattle, WA, USA*. New York, NY: ACM.

Cheng, Yung-Sung, and Bean T. Chen. 2008. *Aerosol Sampler Calibration.* Cincinnati, Ohio: American Conference of Governmental Industrial Hygienists.

Demanega, Ingrid, Igor Mujan, Brett C. Singer, Aleksandar S. Anđelković, Francesco Babich, and Dusan Licina. 2021. "Performance Assessment of Low-Cost Environmental Monitors and Single Sensors Under Variable Indoor Air Quality and Thermal Conditions." *Building and Environment* 187:107415. https://doi.org/10.1016/j.buildenv.2020.107415.

Deutsches Institut für Normung e. V. 1995. *Grundlagen Der Meßtechnik - Teil 1: Grundbegriffe*, no. 1319-1:1995. Berlin: Beuth Verlag GmbH.

Feather, Greg A., and Bean T. Chen. 2003. "Design and Use of a Settling Chamber for Sampler Evaluation Under Calm-Air Conditions." *Aerosol Science and Technology* 37 (3): 261–70. https://doi.org/10.1080/02786820300946.

Hapidin, Dian Ahmad, Casmika Saputra, Dian Syah Maulana, Muhammad Miftahul Munir, and Khairurrijal Khairurrijal. 2019. "Aerosol Chamber Characterization for Commercial Particulate Matter (PM) Sensor Evaluation." *Aerosol Air Qual. Res.* 19 (1): 181–94. https://doi.org/10.4209/aaqr.2017.12.0611.

International Bureau of Weights and Measures. 2008. "International Vocabulary of Metrology: Basic and General Concepts and Associated Terms (VIM)." JCGM 200:2008.

Moreno-Rangel, Alejandro, Tim Sharpe, Filbert Musau, and Gráinne McGill. 2018. "Field Evaluation of a Low-Cost Indoor Air Quality Monitor to Quantify Exposure to Pollutants in Residential Environments." *J. Sens. Sens. Syst.* 7 (1): 373–88. https://doi.org/10.5194/jsss-7-373-2018.

Saleh, Saad Nahi. 2010. "CFD Simulations of a Co-Current Spray Dryer." *Chemical and Molecular Engineering* 4 (2). https://doi.org/10.5281/ZENODO.1084666.

Sayahi, T., D. Kaufman, T. Becnel, K. Kaur, A. E. Butterfield, S. Collingwood, Y. Zhang, P-E Gaillardon, and K. E. Kelly. 2019. "Development of a Calibration Chamber to Evaluate the Performance of Low-Cost Particulate Matter Sensors." *Environmental pollution (Barking, Essex : 1987)* 255 (Pt 1): 113131. https://doi.org/10.1016/j.envpol.2019.113131.

Sturm, Oliver. 2019. "Begleitende Vorlesung Zur Übung Im Mastermodul CFD: (ANSYS Version 19.1)." Skript, Institut für Technische Gebäudeausrüstung, Technische Hochschule Köln.